2008

Impacts of Chromophoric Dissolved Organic Material on Surface Ocean Heating in the Chukchi Sea

Victoria J. Hill
Old Dominion University

Original Publication Citation

Hill, V. J. (2008). Impacts of chromophoric dissolved organic material on surface ocean heating in the Chukchi Sea. *Journal of Geophysical Research: Oceans, 113*(C7), C07024. doi:10.1029/2007jc004119

Impacts of chromophoric dissolved organic material on surface ocean heating in the Chukchi Sea

Victoria J. Hill[1]

Received 22 January 2007; revised 14 November 2007; accepted 5 March 2008; published 18 July 2008.

[1] Recent observations show visible light attenuation in the Arctic Ocean to be greater than previously assumed. High attenuation observed during the period prior to ice melt and increased phytoplankton production, was attributed primarily to the high levels of absorption by chromophoric dissolved organic material (CDOM) present in these waters. Preliminary evidence suggests this material is produced by ice algae in the early spring. Optical data from the Chukchi shelf system collected in the spring and summer of 2002, were used to model energy absorption in the mixed layer by both dissolved and particulate material. In the spring, absorption by CDOM was responsible for increasing the energy absorbed in the mixed layer by 40% over pure seawater. Thus CDOM absorption represents a significant factor in the heating budget of Arctic surface waters. The energy absorbed by CDOM has the potential to account for 48% of the springtime ice melt driven by water column heating. With continued warming, negative feedback due to loss of ice algae habitat could slow down heating effects in the spring. However, terrestrial input of CDOM to the Arctic is postulated to increase due to the release of organic carbon from thawing permafrost. Coupled with the loss of the highly reflective sea ice cover during the spring and summer, CDOM absorption may become increasingly influential in the heating budget of Arctic surface waters.

Citation: Hill, V. J. (2008), Impacts of chromophoric dissolved organic material on surface ocean heating in the Chukchi Sea, *J. Geophys. Res.*, *113*, C07024, doi:10.1029/2007JC004119.

1. Introduction

[2] The optical characteristics of the Arctic Ocean during early spring have historically been considered to be close to those of the clearest natural waters (CNW) [*Smith*, 1973; *Smith and Baker*, 1981], and models predicting heating in the surface waters were based on this assumption [*Perovich and Richter-Menge*, 2000]. However, recent studies of the optical properties in the Arctic Ocean have reported high absorption coefficients, derived mostly from chromophoric dissolved organic material (CDOM) [*Wang et al.*, 2005; *Pegau*, 2002; *Gueguen et al.*, 2005], that are comparable to those observed in lower latitude estuarine regions, such as the Chesapeake Bay [*Barnard et al.*, 1998]. In addition, the magnitude of CDOM absorption in sea ice has been observed to be up to two orders of magnitude greater than that found in the adjacent water column [*Scully and Miller*, 2000]. CDOM absorbs highly in the blue and ultraviolet region of the visible spectrum [*Kirk*, 1994], making it a potentially important factor in the absorption of shortwave visible radiation that leads to the heating of surface waters. Observations of light absorption by CDOM during the Surface Heat Budget of the Arctic experimental (SHEBA) ice camp above the Chukchi Plateau revealed that shortwave radiation absorption was 30% higher in the top 10 m, relative to the clearest natural waters [*Pegau*, 2002].

[3] CDOM is the optically active fraction of the dissolved organic material (DOM) pool which is present in natural waters. However, it should be noted that DOM concentration and the magnitude of absorption by CDOM are only strongly correlated in coastal regions influenced by riverine input [*Blough and Del Vecchio*, 2002]. CDOM is released through the degradation of plant tissue, whether in soils (terrestrial) or in water (freshwater/marine). Terrestrial sources of CDOM absorption tend to dominate in coastal regions influenced by freshwater input, with the underlying in situ source often masked by the high riverine signal [*Blough and Del Vecchio*, 2002]. Marine, or in situ, sources of CDOM include the extracellular release by phytoplankton during active growth [*Vernet and Whitehead*, 1996], and through the destructive forces of zooplankton grazing, viral cell lysis and remineralization of DOM to CDOM by bacteria [*Nelson et al.*, 1998]. The absorption signal from CDOM is removed from marine waters by photochemistry and biodegradation. Excitation by UV radiation can mineralize CDOM to CO_2 and to a lesser extent CO, and degrade refractory high molecular weight compounds to more biologically labile low-molecular-weight compounds [*Moran and Zepp*, 1997]. Newly produced CDOM of marine origin measured in cultures by *Nelson et al.* [2004], appeared to be highly labile and was quickly consumed by bacteria in less

[1]Department of Ocean, Earth and Atmospheric Sciences, Old Dominion University, Norfolk, Virginia, USA.

0148-0227/08/2007JC004119

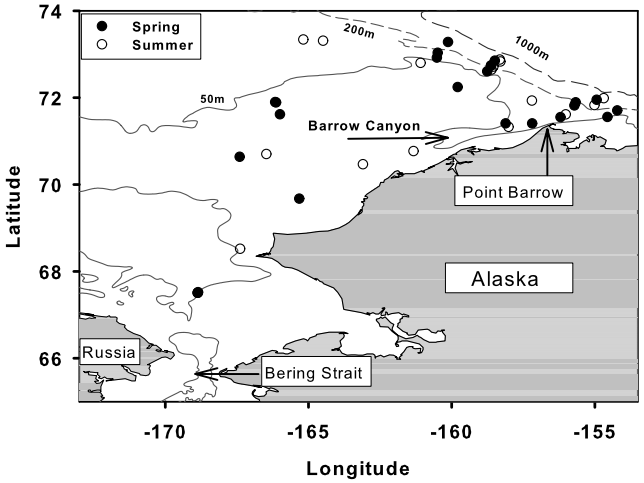

Figure 1. Station locations in the Chukchi Sea. Stations visited in the spring of 2002 are indicated by closed circles, those in the summer of 2002 by open circles.

than 30 d. Material persisting after 50 d escaped rapid decomposition by bacteria, and was considered by *Nelson et al.* [2004] to be part of the refractory pool.

[4] The Arctic environment is undergoing unprecedented changes at a rate faster than the rest of the planet. The warming rate north of 70°N is almost twice that of the temperate and tropical regions [*Hassol*, 2004]. This warming leads to the loss of the highly reflective snow and ice cover, which produces another positive feedback on warming in the area. Estimates put the net annual decrease in sea ice cover at 3% year^{-1} since 1979 (http//www.nsidc.org/data/sezice_index/ [*Serreze et al.*, 2003]), and the summer extent of the ice pack is decreasing annually by approximately 6%. In addition ice thickness has decreased by an average of 1.3 m since the 1960s [*Rothrock et al.*, 1999, 2003]. Reduction in the spatial extent of sea ice can be expected to narrow the window of growth for ice algae, but increase the temporal extent of water column production. On land, a consistent increase in summer surface air temperature [*Chapin et al.*, 2005] has warmed the soils and begun melting the permafrost, greening the Arctic biome and increasing the mobility of terrigenous DOM [*Stokstad*, 2004; *Lawrence and Slater*, 2005; *Zimov et al.*, 2006]. Statistically significant increases in riverine discharge observed during the winter months in the Beaufort, Kara, Laptev, and Bering Seas due to earlier snowmelt [*Peterson et al.*, 2002] would be expected to increase the flux of terrestrial carbon to the coastal ocean. The aim of this study was to quantify the role of CDOM absorption in the heating dynamics of the Arctic mixed layer and estimate its potential impact on sea ice melt.

2. Methods

2.1. Study Area

[5] Data were collected between the 8 May and 12 June 2002 (spring) and 18 July to 21 August 2002 (summer) on the Chukchi shelf (Figure 1). During the spring, ice covered up to 80% of the sea surface. Particulate material in the water column was low with average chlorophyll and suspended material concentrations of <0.5 mg m^{-3} [*Hill and Cota*, 2005], and 0.7 mg/L, respectively. Sea ice was largely absent from the shelf areas during the summer. Surface concentrations of chlorophyll less than 0.1 mg m^{-3} with subsurface maxima of 10 mg m^{-3} were observed, characteristic of postbloom conditions [*Hill and Cota*, 2005].

2.2. Absorption Coefficients

[6] Discrete water samples were collected in 30L Niskin bottles at six light depths corresponding to approximately 100–80, 50, 30, 15, 5 and 1% of surface irradiance. The particulate fraction was collected on Whatman GF/F glass fiber filters (nominal pore size 0.7 μm). The filtrate was collected into clean plastic bottles after a second filtration through a 0.2 μm polycarbonate filter. Experiments using ultrapure deionized water (18 MΩ) shows that there was no significant leaching of optically active material in the wavelength range 300 to 800 nm from the sample bottles into the sample itself. Chlorophyll and phaeopigments concentrations were determined using standard fluorometric methods after extracting the filters in 90% acetone for 24 h at −20°C [*Holm-Hansen et al.*, 1965].

[7] Total particulate spectral absorption coefficients [$a_p(\lambda)$] were measured using the filter pad technique in accordance with current NASA protocols [*Mitchell*, 1990; *Mitchell et al.*, 2002]. A pad moistened with ultrapure deionized water functioned as a blank. The equivalent optical densities (base 10 logarithm) were converted to total particulate [$a_p(\lambda)$] absorption coefficients (natural logarithm) in a suspension, and corrected for multiple scattering amplification according to *Cleveland and Weidemann* [1993]. The average absorption from 790–800 nm was then subtracted to correct for residual nonspecific scattering [*Mitchell et al.*, 2002].

[8] The absorption of the filtrate was measured spectrophotometrically in a 10 cm quartz curvette. Ultrapure deionized water was used for field blanks as per NASA protocols [*Mitchell et al.*, 2002]. The measured spectral absorbances (D) were converted to absorption coefficients: from this point referred to as $a_{CDOM}(\lambda)$.

[9] Total absorption (a_t) was calculated as the sum of a_p and a_{CDOM}. Seawater absorption (a_w) was taken from the measurements of *Pope and Fry* [1997].

2.3. Water Column Energy Absorption

[10] The radiative transfer model *Hydrolight* (Sequoia Scientific Ver 4.2) was used to calculate absorption of visible-near infrared (350 to 800 nm) solar energy by CDOM and particulate matter within the water column. Water column optical properties were parameterized separately for spring and summer conditions using average in-water measurements of chlorophyll concentration, chlorophyll specific phytoplankton absorption [$a_a(\lambda)$*], $a_p(\lambda)$ and $a_{CDOM}(\lambda)$ from bio-optical stations within the study area, for both spring and summer cruises.

[11] To model the separate impacts of absorption by pure water, particulate material and CDOM on radiative absorption in the surface waters of the Chukchi Shelf, *Hydrolight* was parameterized in four configurations: 1. Pure seawater,

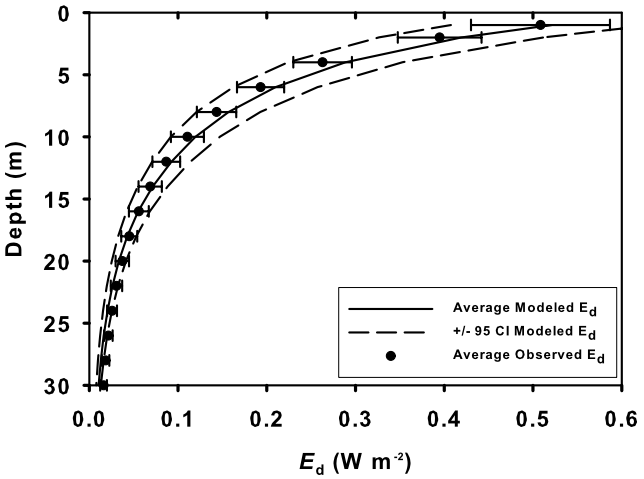

Figure 2. Average profiles of measured and modeled downwelling plane irradiance. Error bars on measured data represent 95% confidence limits. Dashed line represents 95% confidence limits of modeled data.

$a_w(\lambda)$ [*Pope and Fry*, 1997]. 2. $a_w(\lambda) + a_p(\lambda)$. 3. $a_w(\lambda) + a_{CDOM}(\lambda)$. 4. $a_w(\lambda) + a_{CDOM}(\lambda) + a_p(\lambda)$. *Hydrolight* was also parameterized with $a_w(\lambda)$ plus $a_{CDOM}(\lambda)$ values from the Bermuda Atlantic Time series study to provide a low latitude comparison ($a_{CDOM}(355) = 0.077$ m^{-1}, S = 0.025 [*Nelson and Siegel*, 2002]). These a_{CDOM} values were 18% of the a_{CDOM} values observed in the Chukchi Sea. Finally to simulate a future with increased terrestrial CDOM absorption due to warming of permafrost and increased vegetative growth the observed 2002 spring $a_{CDOM}(355)$ values were doubled from 0.38 m^{-1} to 0.76 m^{-1} to approximate a_{CDOM} values observed in the more terrestrially influenced Beaufort Sea [*Gueguen et al.*, 2005].

[12] Atmospheric parameterizations for *Hydrolight* were based on latitude, longitude and local time coincident with radiometric observations from the ship. Simulated cloud cover ranged from 0 to 100% to encompass the range observed in the field. To test the results of the *Hydrolight* simulations, the normalized root mean square difference (RMS), between the simulated downwelling irradiance ($\hat{E}_{d(z)}$) and measured downwelling irradiance ($E_{d(z)}$) was calculated as follows:

$$RMS\% = 100^{*}\sqrt{\frac{\left[\left(\hat{E}_{d(z)} - \hat{E}_{d(z)}\right)/\hat{E}_{d(z)}\right]^2}{n}}$$

Where n is the total number of observations.

[13] The relationship between variation in a_{CDOM}, cloud cover and the resulting energy absorption into the mixed layer was investigated. The model was initialized with a_{CDOM} values between 0.042 and 0.4 m^{-1}, cloud cover simulations were run every 10% between 0% (no cloud cover) and 100% (total cloud cover). The resulting energy absorption in the mixed layer (30 m) was then calculated.

[14] The daily solar radiant flux into the water column was calculated by running the *Hydrolight* simulation at 1 h intervals over the course of 24 h. The area under the curve was then integrated.

3. Results

3.1. Validation of Model Results

[15] The average modeled $\hat{E}_d$ profile (±95% confidence limits) completely overlapped the average and ±95% CL in the observed E_d profiles within the surface mixed layer (0 to 30 m) (Figure 2). The normalized root mean square difference (RMS) between the average profiles of $\hat{E}_d$ and E_d was 15.5%. The model results were statistically consistent with the observed profiles and are suitable for calculating heating absorption by the water column.

3.2. Field Observations of a_{CDOM}

[16] CDOM absorption at 440nm [$a_{CDOM}(440)$] was responsible for approximately 80% of total absorption [$a_t(440)$] in the top 10m of the water column during the spring (Figure 3A). This value decreased to approximately 70% at 30 m. Values of $a_{CDOM}(440)$ at the surface averaged 0.1 m^{-1}, placing them close to values observed in nearshore estuarine regions [*Barnard et al.*, 1998]. During the summer, $a_{CDOM}(440)$ was responsible for approximately 38% of $a_t(440)$ at the surface, where $a_t(440)$ and $a_{CDOM}(440)$ were 34% and 73% of spring values respectively (Figure 3B). The subsurface increase in $a_{CDOM}(440)$ and $a_t(440)$ ob-

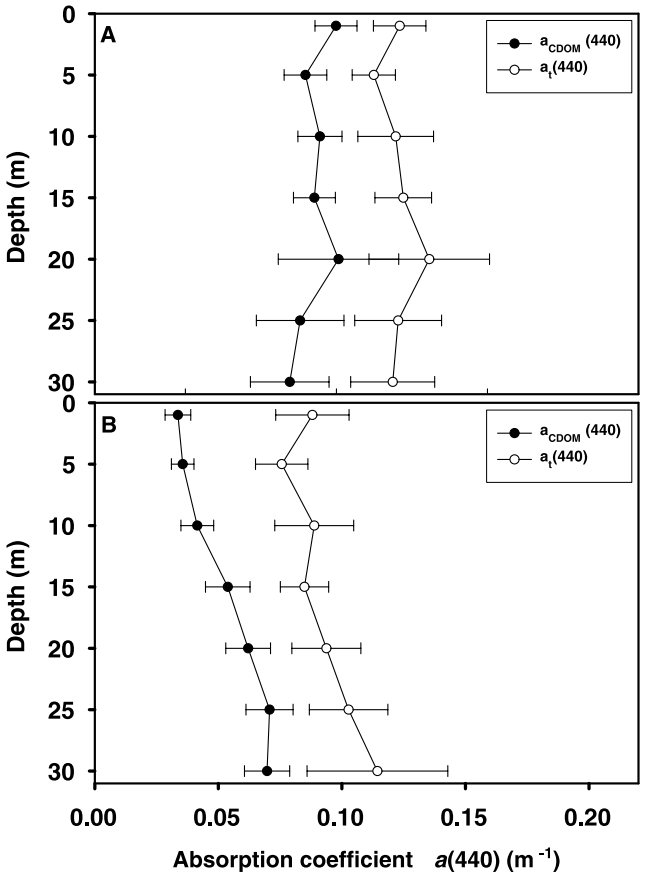

Figure 3. Depth profiles of mean CDOM [$a_{CDOM}(440)$] and total [$a_t = a_w + a_p + a_{CDOM}$] absorption with depth for (A) spring 2002, and (B) summer 2002. Error bars represent ±1 standard error of the mean.

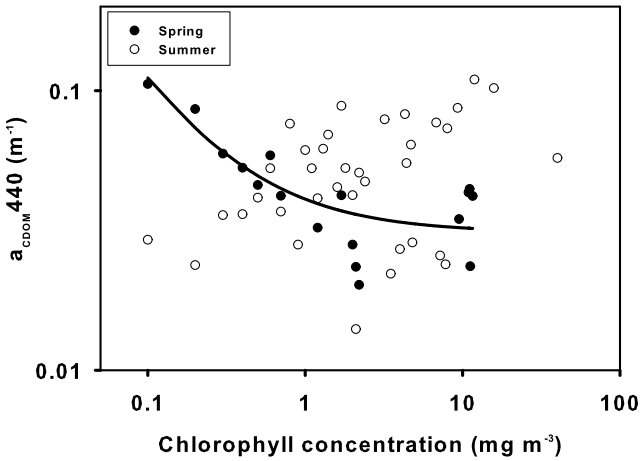

Figure 4. Average $a_{CDOM}(440)$ plotted as a function of chlorophyll concentration in the Chukchi Sea from the spring and summer of 2002. Solid line represents the spring regression (Table 1).

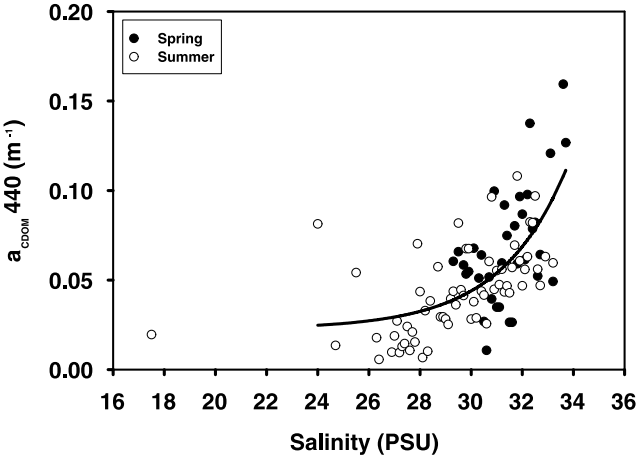

Figure 5. Average $a_{CDOM}(440)$ plotted as a function of salinity in the Chukchi Sea from the spring and summer of 2002.

served during the summer at 20–25 m was associated with an increase in phytoplankton biomass at the top of the halocline [*Hill and Cota*, 2005], summer values were 82% and 96% of the values observed in the spring, and $a_{CDOM}(440)$ contributed 60% of $a_t(440)$.

3.3. Sources of CDOM

[17] The relationship between the average $a_{CDOM}(440)$ observed within each 0.1 mg m^{-3} chlorophyll bin was described by a negative power curve for the spring (Figure 4, $r^2 = 0.83$, $p < 0.01$, Table 1). Thus the highest levels of $a_{CDOM}(440)$ were correlated with the lowest water column chlorophyll concentrations. During the summer no statistical relationship was found between $a_{CDOM}(440)$ and chlorophyll concentration.

[18] In contrast, a weak but statistically significant positive relationship was observed between salinity and average $a_{CDOM}(440)$ for the spring and summer combined (Figure 5, $r^2 = 0.44$, $p < 0.01$, Table 1). The values of $a_{CDOM}(440)$ in the spring (average = 0.066 m^{-1}) were greater than those observed in the summer (average = 0.041 m^{-1}) (ANCOVA, Table 1).

3.4. Impact of CDOM Absorption

3.4.1. Spring

[19] An euphotic depth (1% of surface light) of 200 m was modeled in the pure seawater-only simulation, with 70% of the surface incident light energy absorbed within the mixed layer (upper 30 m) (Figure 6A). The addition of particulate absorption to the model reduced the euphotic zone to 66 m and increased absorption of light energy within the mixed layer (upper 30 m) to 88% of incident. When particulate absorption was replaced by observed levels of $a_{CDOM}(\lambda)$, the euphotic zone was further reduced to 42 m and 97% of surface light was absorbed in the mixed layer (upper 30 m). Adding all absorption coefficients ($a_w + a_p + a_{CDOM}$) to the simulation produced an euphotic zone of 36 m with 98% of all solar radiation being absorbed in the mixed layer. The variance in energy absorbed in the mixed layer due to a 1 standard error change in $a_{CDOM}(\lambda)$ or $a_p(\lambda)$ was 0.5%. Replacing arctic values of $a_{CDOM}(\lambda)$ in the simulation with those from the open ocean station at the Bermuda Atlantic Time series (BATS) increased the depth of the euphotic zone to over 60 m and reduced light energy absorption in the mixed layer by 16% relative to the simulation using water, $a_p(\lambda)$ and $a_{CDOM}(\lambda)$ characteristic of the Chukchi Sea. Absolute magnitudes of energy absorption range from 0.23 MJ h^{-1} for pure seawater in the mixed layer at solar noon, to 0.34 MJ h^{-1} for the water column containing CDOM absorption (Table 2).

3.4.2. Summer

[20] Model results predicted equal contributions from CDOM and particulate matter absorption to energy absorption during the summer (Figure 6B). The fraction of light energy absorbed by the mixed layer from simulations including both particulate and CDOM absorption was

Table 1. Regression Equations for Chlorophyll and Salinity Versus $a_{CDOM}(440)$, Data Displayed in Figures 4 and 5 Respectively[a]

Variable	Equation	a	b	c	r^2	F-Ratio	p
Chlorophyll (spring)	$y = a + bx^c$	0.031	0.00985	−0.91	0.83	34.2	<0.01
Salinity	$y = a + b \exp\left(-x/c\right)$	0.02267	1.99E-07	−2.592	0.44	37.2	<0.01

Source	Sum-of-Squares	DF	Mean Square	F-ratio	p
Cruise	0.067	1	0.067	42.567	<0.01
Error	0.633	401	0.002		

[a]Results of ANCOVA analysis on $a_{CDOM}(440)$ values from spring and summer of 2002.

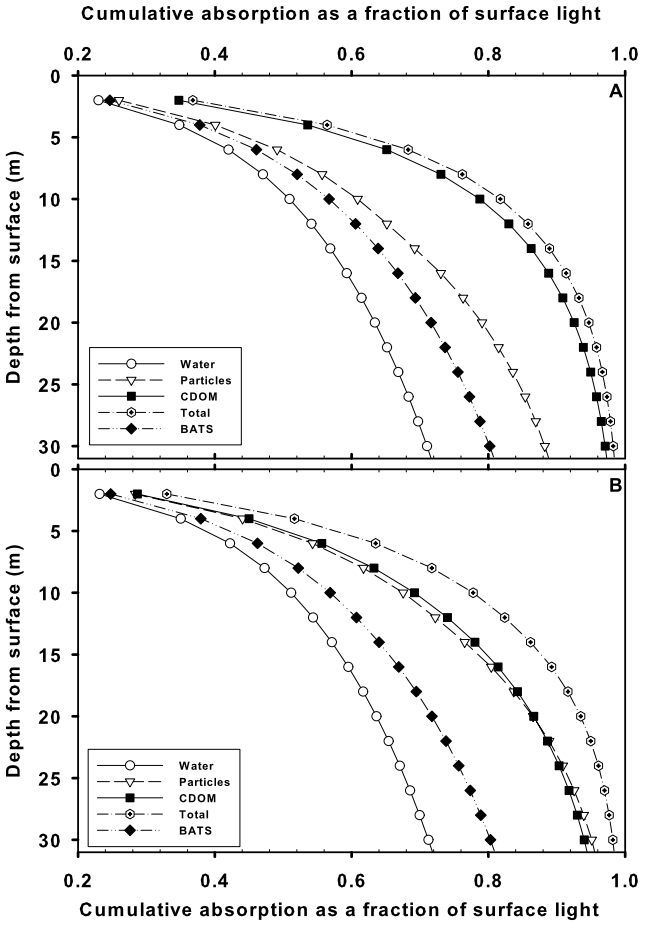

Figure 6. Depth profiles of cumulative energy absorption at 2-m intervals throughout the water column as a fraction of surface light available for the simulations described in the text. (A) spring, (B) summer.

95% relative to 70% absorbed by the pure water simulation. This represented a 10% increase in the fraction of light energy absorbed by particulate material in the mixed layer compared to the spring, but a 3% decrease in the fraction of light energy absorbed by CDOM. A decrease in the solar zenith angle following the summer solstice lowered the surface irradiance by 53% [*Campbell and Aarup*, 1989],

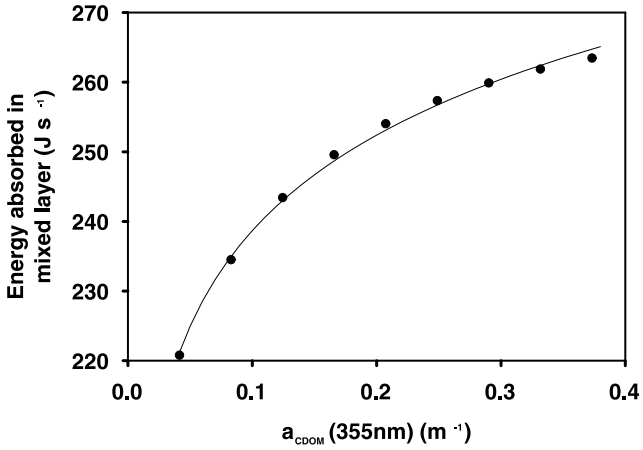

Figure 7. A power curve showing the results of sensitivity testing of the energy absorption model to changes in a_{CDOM}. *Hydrolight* simulations were initialized with successively decreasing a_{CDOM} values from the original observed values and the resultant energy absorbed in the mixed layer calculated.

reducing the potential mixed layer energy absorption compared to the spring (Table 2).

3.4.3. Sensitivity of the Model to Changes in $a_{CDOM}(\lambda)$ and Cloud Cover

[21] The relationship between $a_{CDOM}(440)$ and the absorption of energy in the mixed layer follows a linear equation of the form Y = a + b. ln(X) (Figure 7). Variation in $a_{CDOM}(\lambda)$ on the order of the standard errors observed in the study area (Figure 3), caused a ± 0.4% change in energy absorption in the mixed layer. The equation $Y = a + b. X^3$ is used to describe the decrease in solar energy absorbed in the mixed layer with increasing cloud cover (Figure 8). Cloud cover of 50% produced a 7.3% decrease in mixed layer energy absorption. At 75% cloud coverage, energy absorption in the mixed layer decreased by 30%, and 100% cloud cover reduced energy absorbed in the mixed layer by 75%.

3.5. Impact of CDOM Absorption on Surface Layer Heating

[22] As seen above, $a_{CDOM}(\lambda)$ increased the amount of energy absorbed in the mixed layer of the Chukchi shelf,

Table 2. Rates of Water Column Heating in the Spring and Summer at Solar Noon, Based on the Absorption of Light Energy in the Surface Layer (2 m)[a]

Season		Initial Temp	Pure Seawater	Particles	CDOM	Total	BATS	CDOM Doubling
Spring	Energy absorbed (MJ hr^{-1})		0.23	0.26	0.34	0.36	0.25	0.42
	Potential temperature (°C)	−1.6	−1.49	−1.48	−1.44	−1.43	−1.48	−1.39
	Increase over initial temp (°C)		0.11	0.12	0.16	0.17	0.12	0.21
	% increase over seawater			9%	46%	55%	9%	91%
	% increase over initial		6.88%	7.5%	10%	11%	7.5%	13%
Summer	Energy absorbed (MJ hr^{-1})		0.21	0.25	0.25	0.29	0.22	
	Potential temperature (° C)	−0.77	−0.67	−0.65	−0.65	−0.63	−0.66	
	increase over initial temp (°C)		0.10	0.12	0.12	0.14	0.11	
	% increase over seawater			21%	21%	41%	11%	
	% increase over initial		13%	16%	16%	18%	14%	

[a]Pure water contained no dissolved or particulate material; Particles represents the effects of water and particulate material only; CDOM, water and CDOM; Total represents a water column containing pure water, particles and CDOM; BATS was modeled using field measurements of pure water and $a_{CDOM}(\lambda)$ from the Bermuda Atlantic Time series site [*Nelson et al.*, 1998]. Effects projected from a future doubling of current $a_{CDOM}(\lambda)$ from the Chukchi sea spring of 2002 data set are presented in the last column. The variability in energy absorption due to a one standard error change in the absorption coefficient of CDOM or particles is 0.5%.

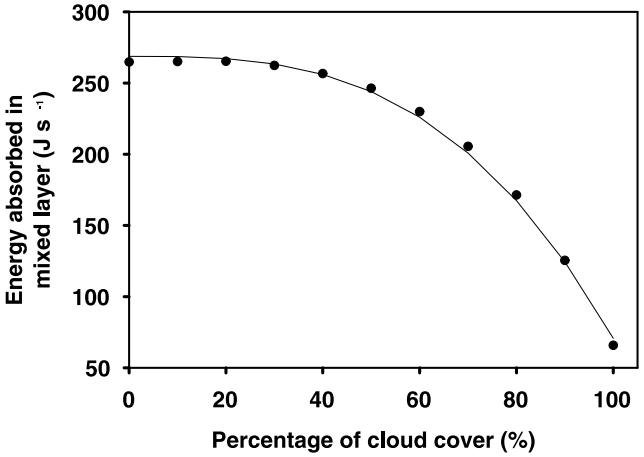

Figure 8. Sensitivity of the energy absorbed to changes in cloud cover. *Hydrolight* simulations were initialized with increasing concentrations of cloud cover and the resultant energy absorbed in the mixed layer calculated.

particularly in the spring. This absorbed energy has the potential to increase the temperature of the water column and accelerate the melting of sea ice. Taking the specific heat of water to be 4.23 KJ Kg^{-1} $Deg^{-1}C$ [*Perovich and Richter-Menge*, 2000], it is possible to estimate the potential temperature increase due to light energy absorption by CDOM and particulate material. A 2 h cloudless heating period around solar noon is used to illustrate this dynamic. Observations of water column temperature give a starting value of −1.6°C and −0.77°C in the spring and summer respectively (Figure 9). The greatest increase in temperature occurs in the upper 10 m, where between 50 to 80 % of incident irradiance is absorbed. In the spring this is the depth range over which the influence of CDOM absorption is most pronounced.

[23] Two hours exposure to the springtime radiant flux centered around solar noon increased the temperature in the top 2 m of a water column containing CDOM absorption by 0.16°C: a 46% increase over solar induced heating of a water column consisting of pure seawater (Figure 9A and Table 2). Absorption by particulate material caused a 0.12°C increase in initial temperature over the same depth, which is a 9% intensification over pure seawater (Figure 9A and Table 2). In the summer, the addition of CDOM or particulate material absorption to pure water both produced a 21% increase in temperature (0.12°C), over pure seawater (0.10°C) (Figure 9B and Table 2). The combined effect of water, CDOM and particulate absorption to total heating in the upper 2 m of the water column would produce a 0.17°C (55%) and 0.14°C (41%) temperature increase in spring and summer respectively.

[24] Using optical characteristics of the clear water environment observed at BATS, modeled heating effects over pure seawater were just 9% in the spring and 11% in the summer. To estimate the potential heating in a future Arctic environment, with increased values of $a_{CDOM}(440)$, a *Hydrolight* simulation was initialized with values double that of the present springtime. The resultant heating effect was a 91% increase over seawater alone [Table 2], and a 0.21°C increase in initial temperature compared to a 0.16°C increase using present-day values.

[25] The absorbed solar energy should promote the melting of sea ice, particularly the lateral melting of leads during the spring. If all energy absorbed by the water column is converted to ice melt, the resulting change in the rate of sea ice melt can be expressed as:

$$\frac{dH}{dT} = \frac{\Delta Fs}{\rho * L}$$

where dH/dT is the rate of ice melt (m s^{-1}), ΔFs (KW m^{-2}) is the increase in heat absorption due to optically active compounds, ρ is the is the density of sea ice (900 kg m^{-3}), and L is the latent heat of fusion of sea ice (300 KJ kg^{-1}).

[26] Using ΔFs calculated from the simulations outlined above, the presence of CDOM absorption in the spring has the potential to increase ice melt by 1.26 mm h^{-1} at solar noon (Table 3). This is a 48% increase over the potential melt in the pure seawater simulation. In comparison ice melt due to energy absorbed by particles was only 0.95 mm h^{-1}. Using the BATS $a_{CDOM}(\lambda)$ for a springtime simulation reduced the rate of ice melt by 28% to 0.91 mm h^{-1}. Modeled ice melt rates increase by 25%, to 1.57 mm h^{-1} in a future with values of $a_{CDOM}(\lambda)$ double that of the current spring. In the summer, potential ice melt for the water column containing CDOM absorption was 0.94 mm h^{-1}

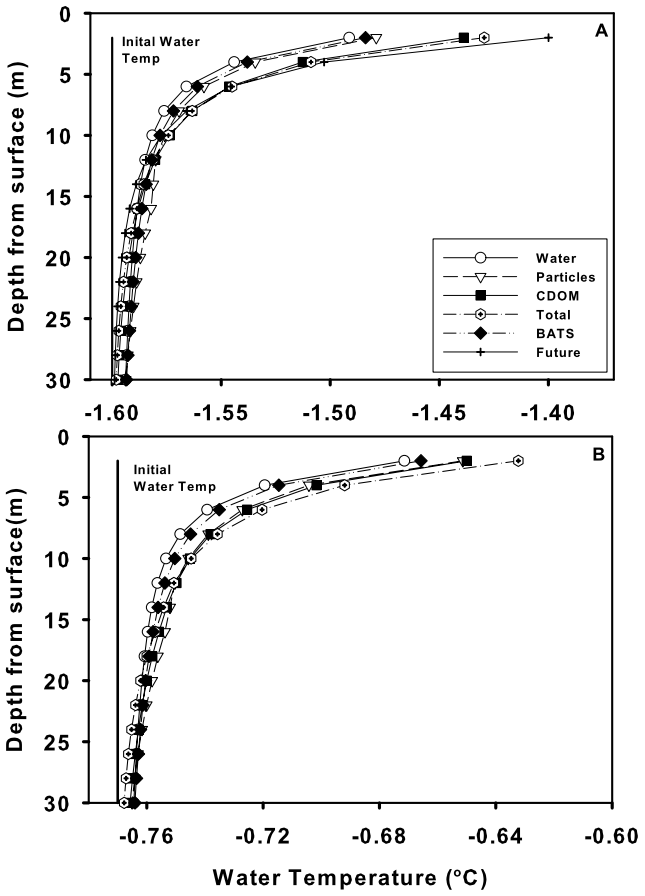

Figure 9. Predicted increase in temperature in the water column for 2 h around solar noon. (A) spring, (B) summer.

Table 3. Rates of Spring Ice Melt Based on the Absorption of Light Energy in the Surface Layer, Calculated in Table 2 and Corrected for Heat Loss to the Atmosphere[a]

	Pure Water	Particles	CDOM	Total	BATS	CDOM Doubling
Potential ice melt, mm h^{-1}	0.85	0.95	1.26	1.34	0.91	1.57
% increase over water		11.4	48	84	6.8	56.9
Heat loss to atmosphere, MJ h^{-1} @ wind speed of 1 mph	0.17	0.17	0.17	0.17	0.17	0.17
Revised ice melt potential, mm h^{-1}	0.22	0.32	0.63	0.71	0.28	0.94

[a]Pure water included no absorption from dissolved other than water or particulate material; ''Particles'' represents the effects of water plus particulate material on light absorption; ''CDOM'' represents the effects of water plus CDOM absorption on light absorption; ''Total'' represents a water column containing pure water, particles and CDOM absorption; BATS was modeled using field measurements of pure water absorption and $a_{CDOM}(\lambda)$ from the Bermuda Atlantic Time series site [*Nelson et al.*, 1998]. Effects projected from a future doubling of current $a_{CDOM}(\lambda)$ from the Chukchi Sea spring of 2002 data set are presented in the last column The variability in potential ice melt due to a 1 standard error change in the absorption coefficient of CDOM or particles is 0.5%.

(Table 4), which is equal to the increase due to energy absorption by particles. However, it should be kept in mind that there was very little ice in the study region at this time.

3.6. Air/Water Heat Flux

[27] Some of the energy absorbed by the surface ocean is lost to the atmosphere in the form of latent (H_L) and sensible heat (H_S) flux. The rate of H_L and H_S depend on the temperature difference between the water and air, as well as wind speed in the case of H_L. A rough estimate of heat loss is possible using the equations of *Andreas and Murphy* [1986]. A lead with a fetch of 100 m was assumed. Observed average daily temperatures of the water surface and air during the spring of −1.6°C and −2.85°C respectively, and in the summer of −0.77°C and −0.25°C, were used. Calculated heat loss from the water surface reduced the potential CDOM absorption induced ice melt to 0.63 mm h^{-1} in the spring (Table 3), and 0.42 mm h^{-1} in the summer (Table 4).

[28] This calculation can also be used to estimate the importance of CDOM absorption in creating a net mixed layer warming effect. A spring time mixed layer consisting of pure seawater absorbed 7.4 MJ d^{-1}. If the combined latent [H_L] and sensible [H_S] heat loss to the atmosphere exceeds this value then a net cooling effect of the mixed layer occurred, i.e.,

$$\text{If } H_{L+}H_S < 7.4 \text{MJd}^{-1} = \text{net heating},$$

$$\text{If } H_{L+}H_S > 7.4 \text{ MJd}^{-1} = \text{net cooling}.$$

[29] Assuming the air and water temperatures of −2.85°C and −1.6°C respectively, then during the spring the combined latent and sensible heat loss to the atmosphere exceeded 7.4 MJ d^{-1} when the wind speed surpassed 6 knots (Figure 10). For the period of field observations in the spring of 2002, 8 d out of 33 had an average wind speed of below 7 knots. Only on these 8 d would a net mixed layer warming occur. With the addition of CDOM absorption into the simulation, energy absorption in the mixed layer increased to 10.7 MJ d^{-1}, increasing the wind speed threshold for net water column heating to 10 knots. Average wind speeds were below 10 knots on 20 of the 33 d, which favored a net warming of the mixed layer.

3.7. Energy Absorption and Heating in the Ice Pack

[30] To provide a comparison between light energy absorption by the ice pack and the water column, the heat flux absorbed by the ice pack and resultant ice melt was calculated using ice albedo and absorption data from the central Arctic Ocean [*Perovich et al.*, 1998]. Surface irradiance was set to the same value as the simulations for water column absorption. Four types of ice were used in the analysis. Cold, snow covered ice is typical of the early spring. Ice covered by melting snow, bare ice and ponded ice are typical of late spring. Ponded ice has the highest absorption characteristics, at 50% of incident light (Table 5). Using the same equations as above to calculate resultant ice melt from energy absorbed within the ice at solar noon, ice melt rates range from 0.33 mm h^{-1} for cold snow covered ice to 1.85 mm h^{-1} for ponded ice. Thus radiative absorption of a CDOM- laden water column produces more ice

Table 4. Rates of Summer Ice Melt Based on the Absorption of Light Energy in the Surface Layer, Corrected for Heat Loss to the Atmosphere[a]

	Water	Particles	CDOM	Total	BATS
Potential ice melt, mm h^{-1}	0.77	0.93	0.94	1.08	0.82
% increase over water		20.4	21.7	39.8	5.78
Heat loss to atmosphere, MJ h^{-1} @ wind speed of 1 mph	0.14	0.14	0.14	0.14	0.14
Revised ice melt potential, mm h^{-1}	0.25	0.41	0.42	0.56	0.30

[a]Pure water contained no dissolved or particulate material; Particles represents the effects of water and particulate material only; CDOM, water and CDOM; Total represents a water column containing pure water, particles and CDOM; BATS was modeled using field measurements of pure water and $a_{CDOM}(\lambda)$ from the Bermuda Atlantic Time series site [*Nelson, et al.*, 1998]. The variance in potential ice melt due to a 1 standard error change in the absorption coefficient of CDOM or particles is 0.5%.

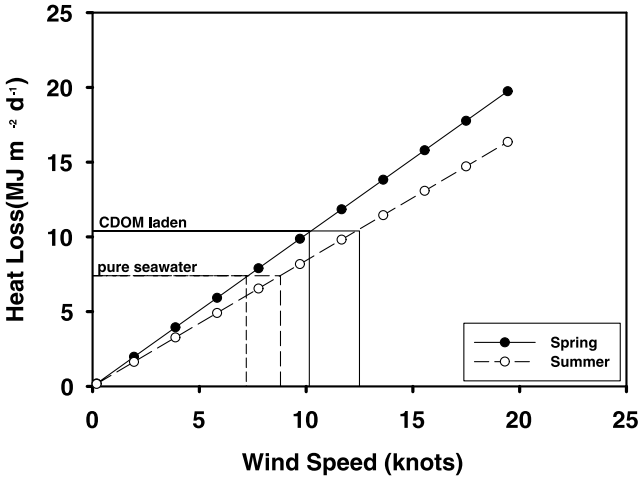

Figure 10. Heat flux to the atmosphere from the sea surface with increasing wind speed, for average water and air temperature of −1.6°C, −2.85°C, and −0.77°C, −0.248°C for spring and summer respectively. The threshold for net water column heating in the pure seawater and CDOM laden water columns also plotted.

melt than direct insolation of dry ice itself, and about as much as bare ice and 30% less than ponded ice.

4. Discussion

4.1. Heating by CDOM

[31] CDOM absorption is instrumental in establishing the optical characteristics of the Chukchi shelf, especially in the early spring. The resulting positive feedback on surface layer heating calculated here has fundamental implications for climate change in the arctic. In the current phase of Arctic warming CDOM absorption increases the energy trapped in the mixed layer, amplifying water column warming and leading to both lateral and bottom ice melt. The melting of sea ice also freshens the surface layer, which increases water column stability and prevents downward mixing of the trapped heat away from the surface. Energy absorbed in the surface layer is also radiated back to the atmosphere enhancing both marine and atmospheric warming.

[32] In addition to solar radiation, heat is transported onto the Chukchi shelf by water advected through the Bering Strait. However, the transit time for this water to the study area is 2 to 12 months [*Woodgate et al.*, 2005]. Consequently the predominant water mass in the study region during ice break up was formed in the Bering Sea and had lost most of its heat during the period of ice formation the previous fall and over the winter. Thus advective transfer does not appear to be a significant source of heat to the region during the spring period of ice melt. This means that solar radiation in the spring is the dominant heating mechanism, making the presence of CDOM absorption critical to the present heating dynamics of the region.

[33] Energy absorbed by the water column is not the only vector for heating that results in ice melt. Direct absorption of solar radiation by the ice pack itself can account for 0.33 to 1.85 mm h^{-1} of ice melt. In comparison, simulated ice melt from energy absorbed by the top 2 m of the CDOM-laden water column was 1.26 mm h^{-1}, of which CDOM absorption is responsible for 48%; the remainder is due to water absorption. Therefore the effective ice melt as a consequence of CDOM absorption in the top 2 m of the water column can exceed that of direct absorption by the ice in the early spring. The implication of this discovery is the importance of CDOM absorption in open leads during the spring, in driving further ice melt.

[34] Open ocean environments are observed to have magnitudes of a_{CDOM} lower than those seen in the Arctic. In the case of the Bermuda Atlantic Time series site a_{CDOM} is only 18% of that found in the Chukchi Sea study area. Simulations of energy absorption using these a_{CDOM} values resulted in mixed layer energy absorption that is only 73% that of Arctic values. This highlights the significant underestimation of the heating effect that will occur when using data from other oceanic regions for Arctic specific issues. Through these results it is evident that the assumptions of clearest natural waters for the Arctic causes large errors in heating budget calculations.

[35] Predictions for climate change in the Arctic include increased vegetative growth, tundra melt and riverine discharge as well as reduced ice cover increasing water column production. These developments can all be expected to increase a_{CDOM} levels in the coastal and central Arctic Ocean. To model the impacts on heating and ice melt dynamics in this future Arctic, simulations were run with double the current a_{CDOM} magnitudes. Simulations increased heating by 91% over pure seawater, a 23% increase over current values of $a_{CDOM.}$ The majority of this heating is in the top 6 m of the water column, which produces an ice melt rate of almost 10 mm h^{-1}, a 25% increase over current a_{CDOM} rates.

4.2. Pan-Arctic Impacts

[36] CDOM absorption coefficients in other regions of the Arctic are similar to those observed in this study (Table 6), indicating that this is not an isolated phenomenon. Measurements from the Labrador Sea and Resolute Bay reveal a_{CDOM} values at 300 nm in the range 0.27–1.18 m^{-1} and 0.32–0.66 m^{-1} respectively. Further north, observations in the North Water Polynya [*Scully and Miller*, 2000] show absorption at 300 nm to range from 0.43–0.66 m^{-1}. Little data are available from the Russian shelf seas, which

Table 5. Ice Melt Rates for Energy Absorbed by the Ice Pack[a]

Ice Type	Albedo, %	Transmission, %	Absorption, %	Ice Melt (mm h^{-1})
Cold snow	0.89	0.02	0.09	0.33
Melting snow	0.8	0.01	0.19	0.69
Bare ice	0.58	0.02	0.4	1.45
Ponded ice	0.35	0.14	0.51	1.85

[a]Ice absorption characteristics from *Perovich et al.* [1998]. Surface irradiance calculated for solar noon during the spring at 272.6 W m^{-2}.

Table 6. Observations of $a_{CDOM}(300)$ From the Arctic for Water and Ice Core Samples[a]

Region	Type	$a_{CDOM}(300)$, m^{-1}	Season	Year
Chukchi Sea	water	0.88 (0.69–1.10)	Spring	2002, 2004
Chukchi Sea	water	0.85 (0.51–1.29)	Summer	2000, 2002, 2004
Central Arctic[a]	water	0.57	Summer	1998
North Water Polynya[b]	water	0.59 (0.43–0.66)	May	1998
Resolute Bay	water	0.53 (0.27–1.18)	Summer	1994, 1998
Labrador Sea	water	0.49 (0.32–0.66)	Jul/Aug	1996, 1997
Southern Ocean[c]	water	0.351 (0.14–8.78 (extreme)		
North Water Polynya[b]	ice	7.27 (1.12–34.39)	May	1998
Resolute Bay[c]	ice	(7–11)	Aug	1998

[a] *Pegau* [2002].
[b] *Scully and Miller* [2000].
[c] *Reynolds et al.* [2001].

are heavily influenced by riverine input [*Gordeev*, 1998]. Thus $a_{CDOM}(\lambda)$ could be even more pronounced in these regions. Warming of the Arctic has already increased riverine discharge [*Peterson et al.*, 2002] and promoted the widespread melting of permafrost which mobilizes organic carbon trapped in the sediments [*Stokstad*, 2004]. These processes, along with the growth of terrestrial vegetation are likely to accelerate with continued warming [*Myneni et al.*, 1997; *Tucker et al.*, 2001]. All of these processes can be expected to intensify CDOM input to the Arctic Ocean, thereby amplifying the CDOM heating signal. A further simulation using a_{CDOM} values double that observed in the Chukchi sea during the spring of 2002, was utilized to project the results of increased CDOM absorption. Although the fraction of incident light absorbed in the mixed layer did not increase significantly from current day values, the intensity of heating in the top 2 m increased by ~20% (Figure 7A) with a corresponding increase in ice melt rates. This also increased the energy trapped in the upper layer of the water column, which is then available to be reradiated back into the atmosphere contributing to warming.

4.3. What is the Source of CDOM to the Chukchi Sea?

[37] High CDOM absorption signals in coastal waters are usually derived from riverine inputs which typically produce a significant negative relationship with salinity [*Blough and Del Vecchio*, 2002]. Although the relationship with salinity presented here was weak ($r^2 = 0.44$, Table 1), the slope was positive and the highest CDOM absorption values were associated with the highest salinities. A negative relationship between salinity and a_{CDOM} that often indicates conservative mixing of terrestrial sources was not found in this region. Riverine discharge reaches a maximum at the end of May, as ice melt in rivers progresses. Water from the rivers discharging into the Beaufort Sea is unlikely to have a large influence on the Chukchi shelf, as the Chukchi is the dominant source of seawater to the Beaufort, with little flow in the reverse. Water from the Yukon River flows into the Bering Sea and takes approximately 4–6 months to arrive in the northern Chukchi [*Woodgate et al.*, 2005]. Given the length of time for transport of water masses onto the Chukchi shelf, terrestrial sources of CDOM absorption would not be expected to peak until the summer [*Woodgate et al.*, 2005] Thus riverine input does not appear to be the main driver of high CDOM absorption levels in the area of the Chukchi shelf studied here. The marine source of the CDOM absorption, however, appears enigmatic. CDOM absorption was highest in the early spring, associated with low chlorophyll concentrations throughout the water column, and declined as phytoplankton concentration increased in the summer. This suggests that the CDOM absorption signal was not a product of algal bloom formation in the water column. The answer may lie in high magnitudes of CDOM absorption recorded in sea ice cores from other regions of the Arctic. In these cases CDOM absorption in the ice was up to two orders of magnitude greater than in the water column beneath [*Scully and Miller*, 2000]. Previous experimentation has shown that DOC (of which CDOM is a component) is incorporated conservatively into sea ice during formation [*Giannelli et al.*, 2001]. However, the production of DOC in sea ice has been observed to be highly correlated to ice algae biomass [*Smith et al.*, 1997]. This suggests that sea ice acts as a mechanism for concentrating CDOM after formation over the winter and as ice algal production commences in the spring. The breakup of surface ice releases the material into the surface waters, initiating the heating feedback loop. CDOM is then consumed by photo-oxidation and biodegradation.

[38] The source of CDOM into the Arctic Ocean and the resulting pathway of degradation is important when we consider the timescales over which CDOM absorption has a significant effect on the heat budget. Newly produced, highly labile material may only be present for a few days [*Nelson et al.*, 2004] in which case the increase in energy absorption due to this material is short-lived. If most of the spring time CDOM absorption is in fact from ice algae and is labile, then the CDOM induced increase in heating will only last until open water allows for wide scale photodegradation to occur. In the spring, this timescale is a matter of weeks. Refractory material which persists in the environment over seasonal timescales will affect the heat budget well into the summer.

4.4. Sea Ice: CDOM Coupling

[39] Sea ice appears to act as a focusing mechanism for CDOM absorption, concentrating it in the surface waters where the impact of heating is most pronounced. The evidence presented here indicates that this coupling of sea ice and CDOM absorption is crucial in the current heating dynamics of the Arctic, but will be disrupted due to accelerated climate change in the area. Possible scenarios include the continued reduction in the extent of wintertime sea ice coupled with earlier sea ice melt. This leads to less CDOM incorporation into winter sea ice and a reduction in

the length of the ice algae production window. The result is a negative feedback on ice melt, as CDOM absorption in the surface waters in early spring is reduced. This may slow down the acceleration of sea ice melt for some period of time. Superimposed on changes in the production and storage of CDOM from in situ sources, is the possibility of an increase in the input of terrestrial CDOM, that will further enhance the warming of the Arctic system.

[40] Clearly CDOM absorption plays an instrumental role in the dynamics of the heating budget in the Arctic Ocean. Consequently, the presence of this material must be taken into consideration in any modeling efforts in the Arctic that include a heating factor from solar radiation. However, the primary sources of CDOM absorption in sea ice and the surface waters of the Arctic remain unknown as do the impacts on this composition on climate change, the length of time that the high CDOM absorption values are present once sea ice has retreated from an area, and feedbacks between CDOM absorption and spring surface heating and how they impact and can be impacted by climate change.

[41] **Acknowledgments.** The author thanks D.A. Ruble, X. Pan, J. Wang and Z.-P. Mei for assistance in data collection. The author is also grateful to R. Zimmerman for discussions and comments on the manuscript. This work was supported by the National Research Foundation Office of Polar Programmes, as part of the Western Arctic Shelf Basin Interactions Project, grant OPP-0125049.

References

Andreas, E. L., and B. Murphy (1986), Bulk transfer coefficients for heat and momentum over leads and polynyas, *J. Phys. Oceanogr.*, *16*, 1875–1883.

Barnard, A. H., W. S. Pegau, and R. V. Zaneveld (1998), Global relationships of the inherent optical properties of the oceans, *J. Geophys. Res.*, *103*, 24,955–24,968.

Blough, N. V., and R. Del Vecchio (2002), Chromophoric DOM in the coastal environment, in *Biogeochemistry of Marine Dissolved Organic Matter*, edited by D. Hansell and A. C. A. Carlson, pp. 509–546, Elsevier, San Diego, Calif.

Campbell, J. W., and T. Aarup (1989), Photosynthetically available radiation at high latitudes, *Limnol. Oceanogr.*, *34*, 1490–1499.

Chapin, F. S., et al. (2005), Role of land-surface changes in Arctic summer warming, *Science*, *310*, 657–660.

Cleveland, J., and S. A. D. Weidemann (1993), Quantifying absorption by aquatic particles: A multiple scattering correction for glass-fiber filters, *Limnol. Oceanogr.*, *38*, 1321–1327.

Giannelli, V., D. N. Thomas, C. Haas, G. Kattner, H. Kennedy, and G. S. Dieckmann (2001), Behaviour of dissolved organic matter and inorganic nutrients during experimental sea-ice formation., *Ann. Glaciol.*, *33*, 317–321.

Gordeev, V. V. (1998), River input of water, sediment, major ions, nutrients and trace metals from Russian territory to the Arctic Ocean, in *The Freshwater Budget of the Arctic Ocean*, edited by E. L. Lewis, pp. 297–322, Springer, New York.

Gueguen, C., L. Guo, and N. Tanaka (2005), Distributions and characteristics of coloured dissolved organic matter in the western Arctic Ocean, *Cont. Shelf Res.*, *25*, 1195–1207.

Hassol, S. J. (2004), *ACIA, Impacts of a Warming Arctic: Arctic Climate Impact Assessment*, Cambridge Univ. Press, Canada.

Hill, V., and J. G. F. Cota (2005), Spatial patterns of primary production on the shelf, slope and basin of the western arctic in 2002, *Deep Sea Res., Part II*, *52*, 3344–3354.

Holm-Hansen, O., C. J. Lorenzen, R. W. Holmes, and J. D. H. Strickland (1965), Fluorometric determination of chlorophyll, *ICES J. Mar. Sci.*, *30*, 3–15.

Kirk, J. T. O. (1994), *Light and Photosynthesis in Aquatic Ecosystems*, Cambridge Univ. Press, Cambridge, U.K.

Lawrence, D. M., and A. G. Slater (2005), A projection of severe near-surface permafrost degradation during the 21st century, *Geophys. Res. Lett.*, *32*, L24401, doi:10.1029/2005GL025080.

Mitchell, B. G. (1990), Algorithms for determining the absorption coefficient of aquatic particulates using the quantitative filter technique (QFT), in *Ocean Optics X*, pp. 137–148, The Int. Soc. for Opt. Eng., Ocean Optics, Bellingham, Wash.

Mitchell, B. G., M. Kahru, J. Wieland, and M. Stramska (2002), Determination of spectral absorption coefficients of particles, dissolved material and phytoplankton for discrete water samples, in *Ocean Optics Protocols for Satellite Ocean Color Sensor Validation*, edited by J. Mueller and L. G. S. Fargion, pp. 231–257, NASA, Hanover, Germany.

Moran, M. A., and R. G. Zepp (1997), Role of photoreactions in the formation of biologically labile compounds from dissolved organic matter, *Limnol. Oceanogr.*, *42*, 1307–1316.

Myneni, R. B., C. D. Keeling, C. J. Tucker, G. Asrar, and R. R. Nemani (1997), Increased plant growth in the northern high latitudes from 1981 to 1991, *Nature*, *386*, 698–702.

Nelson, N. B., and D. Siegel (2002), Chromophoric DOM in the open ocean, in *Biogeochemistry of Marine Dissolved Organic Matter*, edited by D. Hansell and A. C. A. Carlson, pp. 547–578, Elsevier, London.

Nelson, N. B., D. Siegel, and A. Michaels (1998), Seasonal dynamics of coloured dissolved material in the Sargasso Sea, *Deep Sea Res., Part I*, *45*, 931–957.

Nelson, N. B., C. A. Carlson, and D. Stephenson (2004), Production of chromophoric dissolved organic matter by Sargasso Sea microbes, *Mar. Chem.*, *89*, 273–287.

Pegau, W. S. (2002), Inherent optical properties of the central Arctic surface waters, *J. Geophys. Res.*, *107*(C10), 8035, doi:10.1029/2000JC000382.

Perovich, D. K., and J. A. Richter-Menge (2000), Ice growth and solar heating in springtime leads, *J. Geophys. Res.*, *105*, 6541–6548.

Perovich, D. K., C. S. Roesler, and W. S. Pegau (1998), Variability in Arctic sea ice optical properties, *J. Geophys. Res.*, *103*, 1193–1208.

Peterson, B. J., R. M. Holmes, J. W. McClelland, C. J. Vorosmarty, R. B. Lammers, A. L. Shiklomanov, I. A. Shiklomanov, and S. Rahmstorf (2002), Increasing river discharge to the Arctic Ocean, *Science*, *298*, 2171–2173.

Pope, R., and M. E. S. Fry (1997), Absorption spectrum (380–700 nm) of pure water. part II: Integrating cavity measurements, *Appl. Optics*, *36*, 8710–8723.

Reynolds, R. A., D. Stramski, and B. G. Mitchell (2001), A chlorophyll-dependent semianalytical reflectance model derived from field measurements of absorption and backscattering coefficients within the Southern Ocean, *J. Geophys. Res.*, *106*(C4), 7125–7138.

Rothrock, D. A., Y. Yu, and G. A. Maykut (1999), Thinning of the Arctic sea-ice cover, *Geophys. Res. Lett.*, *26*, 3469–3472.

Rothrock, D. A., J. Zhang, and Y. Yu (2003), The arctic ice thickness anomaly of the 1990's: A consistent view from observations and models, *J. Geophys. Res.*, *108*(C3), 3083, doi:10.1029/2001JC001208.

Scully, N., and M. W. L. Miller (2000), Spatial and temporal dynamics of colored dissolved organic matter in the north water polynya, *Geophys. Res. Lett.*, *27*, 1009–1011.

Serreze, M. C., J. A. Maslanik, T. A. Scambos, F. Fetterer, J. Stroeve, K. Knowles, C. Fowler, S. Drobot, R. G. Barry, and T. M. Haran (2003), A record minimum arctic sea ice extent and area in 2002, *Geophys. Res. Lett.*, *30*(3), 1110, doi:10.1029/2002GL016406.

Smith, R. C. (1973), Optical properties of the Arctic upper water, *Arctic*, *26*, 303–313.

Smith, R. C., and K. S. Baker (1981), Optical properties of the clearest natural waters, *Appl. Optics*, *20*, 177–184.

Smith, R. E. H., M. Gosselin, S. Kudoh, B. Robineau, and S. Taguchi (1997), DOC and its relationship to algae in bottom ice communities, *J. Mar. Syst.*, *11*, 71–80.

Stokstad, E. (2004), Defrosting the carbon freezer of the north, *Science*, *304*, 1618–1620.

Tucker, C. J., D. A. Slayback, J. E. Pinzon, S. O. Los, R. B. Myneni, and M. A. Taylor (2001), Higher Northern Latitude NDVI and growing season trends from 1982 to 1999, *Int. J. Biometeorol.*, *45*, 184–190.

Vernet, M., and K. Whitehead (1996), Release of ultraviolet-absorbing compounds by the red-tide dinoflagellate, Lingulodinium Polyedra, *Mar. Biol.*, *127*, 35–44.

Wang, J., G. F. Cota, and D. A. Ruble (2005), Absorption and backscattering in the Beaufort and Chukchi Seas, *J. Geophys. Res.*, *110*, C04014, doi:10.1029/2002JC001653.

Woodgate, R. A., K. Aagaard, and T. R. Weingartner (2005), A year in the physical oceanography of the Chukchi Sea: Moored measurements from autumn 1990–1991, *Deep Sea Res., Part II*, *52*, 3116–3149.

Zimov, S. A., E. A. G. Schuur, and F. S. Chapin (2006), Permafrost and the global carbon budget, *Science*, *312*, 1612–1613.

V. J. Hill, Department of Ocean, Earth and Atmospheric Sciences, Old Dominion University, Room 406, 4600 Elkhorn Avenue, Norfolk, VA 23529, USA. (vhill@odu.edu)